JOURNAL OF Materials CHEMISTRY

Growth of multi-walled carbon nanotubes on mechanical alloying-derived Al_2O_3–Ni nanocomposite powder

Binghai Liu,[a] Ziyi Zhong,[b] Jun Ding,*[a] Jianyi Lin,[b] Y Shi[a] and L. Si[a]

[a]*Department of Materials Science, Faculty of Science, National University of Singapore, Singapore 119260*
[b]*Department of Physics, Faculty of Science, National University of Singapore, Singapore 119260*

Received 23rd April 2001, Accepted 19th June 2001
First published as an Advance Article on the web 8th August 2001

Mechanical alloying was employed to produce the nanocomposite Al_2O_3–Ni. It was found that the mechanical alloying of a mixture of NiO and α-Al_2O_3 generated a highly disordered structure. Reduction under a hydrogen atmosphere led to formation of nano-sized Ni crystallites in the Al_2O_3 matrix. Relatively high BET specific surface areas indicate that the sub-micron nanocomposite particles have a porous structure. In comparison with the co-precipitated powder, the mechanical alloying-derived powder shows smaller particle/agglomerate size and much higher Ni reducibility. Multi-walled carbon nanotubes with a high production yield were successfully synthesized by using the mechanical alloying-derived nanocomposite as the catalyst.

Introduction

Since the 1980's, carbon nanotubes (CNTs) have been attracting intensive attention worldwide owing to their unique physical and chemical properties. This new class of low dimensional materials are promising candidates for applications such as catalysts,[1] storage of hydrogen and other gases,[2] biological cell electrodes,[3] nanoscale electronic[4] and mechanical[5] devices, and scanning probe microscope and electron field emission tips.[6,7]

Many techniques have been developed to synthesize CNTs, such as arc-discharge, laser ablation and catalytic methods. Arc-discharge and laser ablation are well-known as techniques which can produce relatively thin and straight CNTs and thus are widely used for synthesizing single-walled nanotubes. However, these methods suffer from low productivity and difficulty in purification of CNT products.[8] Catalytic methods appear quite promising owing to the ready availability of raw materials and low cost, as well as significantly higher productivity, although the techniques generally lead to multi-walled CNTs.

To obtain high-quality CNT products by chemical catalytic routes, one of the key processes is to produce sufficiently small metallic particles, which are active enough for the formation of CNTs.[9] Wet-chemical processes, such as sol–gel[8] and co-precipitation,[9,10] are widely used for the preparation of nanocomposite catalysts. Of these chemical methods, the most noteworthy is the selective hydrogen reduction of oxide solid solution.[9–11] In the resultant nanocomposite materials, the metallic particles were reported to be generally smaller than 10 nm in diameter and located both inside and at the surface of the matrix.[10] Homogeneously dispersed single-walled and multi-walled CNTs were produced when the nanocomposite was used as the catalyst.[9–15]

As is well known, high-energy mechanical milling (or mechanical alloying) is a powerful tool for the production of ultrafine powders and nanocrystalline and nanocomposite materials.[16–19] In this work, we employed mechanical alloying as an alternative to wet chemical methods to produce an Al_2O_3–Ni nanocomposite. Carbon nanotubes were synthesized using the mechanical alloying-derived nanocomposites. In comparison, co-precipitation was also used for synthesizing an Al_2O_3–Ni nanocomposite.

Experiments

A mixture of α-Al_2O_3 powder (Fluka, 99%) and NiO powder (Fluka, 99%) at a weight ratio of 4 : 1 was mechanically milled using a Spex 8000 high-energy shaker mill. Two batches of Al_2O_3–NiO powders were obtained after milling for 18 and 36 h, denoted MA18 and MA36, respectively. The as-milled MA18 and MA36 powders were reduced at different temperatures (300, 450, 600 and 700 °C) for 40 min in a flow of H_2. Following the H_2 reduction, the Al_2O_3–Ni powders were used as catalysts for the growth of carbon nanotubes (CNTs), which were synthesized at 600 °C in CH_4 with a flow rate of 30 ml min^{-1}.

For comparison, another batch of Al_2O_3–NiO precursor was synthesized by co-precipitation of $Al(NO_3)_3{\cdot}9H_2O$ (Fluka, 99%) and $Ni(NO_3)_2{\cdot}6H_2O$ (Fluka, 99%) at a molar ratio of 5.9 : 1 (corresponding to a weight ratio of 4 : 1 of Al_2O_3 to NiO). The obtained precipitates were dried at 80 °C in air and calcined at 700 °C for 3 h to decompose the nitrates. The reduction of the precursor was conducted at 300, 450, 600 and 700 °C in H_2. The nanocomposite powder reduced at 450 °C was used for the catalytic reaction under the same conditions as for the mechanically alloyed powders, namely at 600 °C in CH_4 with a flow rate of 30 ml min^{-1}.

The phase composition of the mechanically alloyed and the co-precipitation-derived precursors, as well as the as-reduced Al_2O_3–Ni nanocomposites, was examined by X-ray diffraction (Philips PW 1820 diffractometer with Cu-Kα radiation). In addition, XRD analysis was also employed to estimate the average grain size of Ni particles in the Al_2O_3–Ni nanocomposites. Magnetic measurements were carried out using a superconducting vibrating sample magnetometer (Oxford Instruments) at room temperature, in order to monitor the formation of magnetic Ni after reduction of NiO. The magnetic measurements were also used to evaluate the carbon content of the CNT-containing nanocomposite powders. The saturation magnetization of as-reduced Al_2O_3–Ni nanocomposites (M_{RS}) and CNT-containing nanocomposite powders (M_{CNT}) was measured at the maximum magnetic field of 20 kOe.

The morphologies of the as-reduced Al_2O_3–Ni powders and the CNT products after catalytic reactions were studied by field-emission scanning electron microscopy (FE-SEM, JEOL-100 CX) and transmission electron microscopy (TEM,

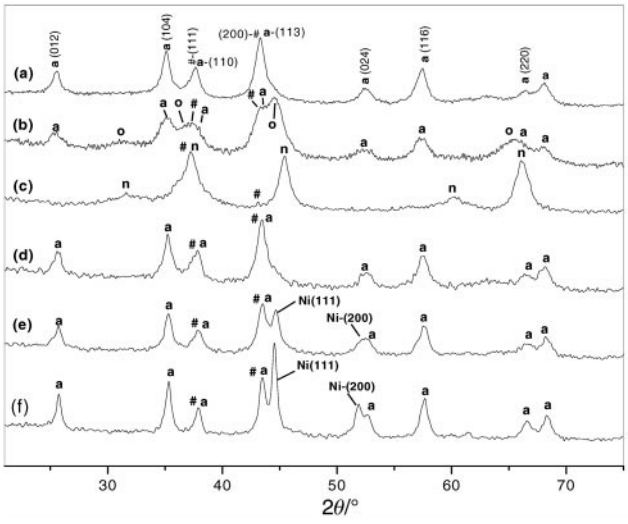

Fig. 1 XRD patterns of oxide precursors and the as-reduced Al_2O_3–Ni composite powders: (a) Al_2O_3–NiO powder milled for 18 h; (b) Al_2O_3–NiO powder milled for 36 h; (c) co-precipitation-derived Al_2O_3–NiO powder; (d) MA36 reduced at 300 °C; (e) MA36 reduced at 450 °C; (f) MA36 reduced at 700 °C (**a**: α-Al_2O_3; **#**: NiO; **o**: $NiAl_2O_4$; **n**: η-Al_2O_3).

JEM-100CX). The Brunauer–Emmett–Teller (BET, Quantochrome Nova 2000) method, using N_2 adsorption at liquid N_2 temperature, was employed to check the change in the specific surface area of the catalytic powders after reduction (S_r) and after catalytic growth of CNTs (S_{CNT}).

Results and discussion

X-Ray diffraction examination

Fig. 1(a) and (b) show the XRD patterns of the MA18 and MA36 Al_2O_3–NiO powders after mechanically alloying for 18 and 36 h, respectively. After mechanical milling for 18 h, broadened peaks appeared, while after 36 h, the NiO(220) peak became undetectable. In comparison with the X-ray diffraction pattern of the MA18 precursor, the diffraction peaks of the MA36 precursor are much broader. A few additional peaks appeared in the ranges 31–32, 36–38, 44–45 and 65–67°. These additional peaks indicate the formation of a new structure/phase, a solid solution of nickel aluminium oxide $NiAl_2O_4$. It can be readily understood that non-equilibrium structures (amorphous and metastable phases) have often been observed in materials after mechanical alloying.[16–21] For the co-precipitation derived precursor, after calcination at 700 °C for 3 h, XRD analysis reveals the formation of η-Al_2O_3 and NiO phases, as shown in Fig. 1(c).

As can be seen from Fig. 1(d), the Ni(111) peak is not obvious for MA36-derived Al_2O_3–Ni powders after reduction at 300 °C, indicating that no significant amount of NiO was reduced to metallic Ni. When the reduction temperature is raised to 450 and 700 °C, the increase in the intensity of the Ni(111) peak can be clearly observed [Fig. 1(e) and (f)], indicating an increase in the amount of Ni. All the diffraction peaks of α-Al_2O_3 and metallic Ni were broadened, indicating that the powders resulting from reduction have a nanocomposite structure. Similar results were observed for the co-precipitation-derived and MA18 powders. Therefore, only the XRD spectra of MA36-derived catalytic powders after reduction are shown here.

In addition, from the X-ray diffraction peaks, we calculated the Ni particle size for different catalytic powders by using the Scherrer formula and the results are shown in Table 1. The superposition of the Ni(111) and α-Al_2O_3(104) peaks may limit the accuracy of the estimation of the mean grain size of the Ni particles. However, the results still enable us to draw the conclusion that mechanical alloying can produce suitable Al_2O_3–Ni catalytic nanocomposites, which may be promising candidates for CNT growth catalysts.

Table 1 Average grain size (R) of Ni particles in Al_2O_3–Ni composite powders reduced at different temperatures

Reduction temperature/°C	MA18-derived catalyst, R/nm	MA36-derived catalyst, R/nm	Co-precipitation-derived catalyst, R/nm
450	10.20	8.13	8.01
700	13.41	12.04	11.80

Magnetic characterization

The formation of magnetic Ni from paramagnetic NiO can be monitored by magnetic measurements. Saturation magnetization (M_s) is shown in Fig. 2 as a function of reduction temperature for MA18 and MA36 powders in comparison with the co-precipitation-derived precursor. For the as-milled MA18 and MA36 powders and the co-precipitated precursor, M_s is below 0.5 emu g^{-1}, corresponding to paramagnetic NiO. After reduction at 300 °C, all the samples show small values of M_s, indicating that only a small amount of Ni was formed. With rising temperatures, the materials obtained by milling methods clearly show higher reducibility. Considering $M_s = 55$ emu g^{-1} for pure Ni, the expected saturation magnetization is approximately 10 emu g^{-1} from the weight ratio $NiO : Al_2O_3 = 1 : 4$. It can be seen from Fig. 2 that after heating at 600–700 °C, the reduction process is almost complete. However, the co-precipitated precursor shows a much lower reducibility. Only approximately 50% of the NiO was converted into Ni after reduction at 700 °C.

Scanning electron microscopic (SEM) study

Fig. 3 shows SEM micrographs of the co-precipitated and mechanically alloyed powders after reduction at 700 °C. The co-precipitation-derived precursor appears as relatively large agglomerates under electron microscopy, as shown in Fig. 3(a). Such microstructure is typical for co-precipitated precursors. Smooth and dense surface morphology is observed, suggesting the occurrence of sintering. As a result, the formation of such large particles results in the entrapment of much of the NiO, and thus hinders the further penetration of H_2 during the reduction. Thus the low reducibility of the co-precipitated precursors was only to be expected.

While agglomerates exist in the mechanically alloyed powders such as MA36, shown in Fig. 3(b), their size is small (typically 100–200 nm) and the structure is rather loose and porous. This can be ascribed to the fact that MA18 and

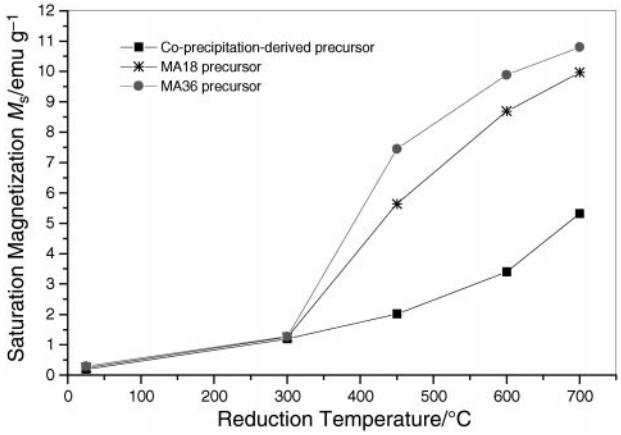

Fig. 2 The dependence of M_s (saturation magnetization) of Al_2O_3–Ni powder on the reduction temperature.

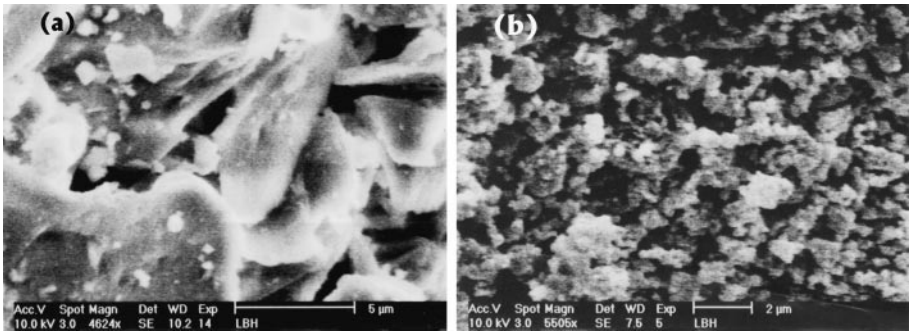

Fig. 3 SEM photographs of Al_2O_3–Ni composite powders obtained from (a) co-precipitation-derived precursor and (b) MA36 precursor.

MA36 only underwent the thermal treatment for 40 min during H_2 reduction and no pre-calcination treatment was conducted. Therefore, the loose structure of the agglomerates provides favorable paths for H_2 penetration, resulting in a greatly accelerated reduction progress. In addition, mechanical alloying results in a nanocomposite mixture with a very fine grain structure. The high density of grain boundaries may promote the diffusion of hydrogen. As shown in Fig. 2, the reducibility of MA36 is higher than that of MA18, indicating that a longer milling time can speed up the reduction process. The higher reducibility of MA36 powder can be ascribed to the formation of $NiAl_2O_4$ solid solution and the further refinement of NiO after mechanical milling for a longer time.

TEM analysis

Fig. 4 shows TEM photographs of the reduced Al_2O_3–Ni composite powders derived from the precursor MA36. The as-milled powder shows a similar amorphous structure; no NiO grains or Al_2O_3–Ni grain boundaries can be seen clearly. This result confirms that the mechanical alloying results in a highly disordered structure, as discussed for Fig. 1. After reduction at 300 °C, a few crystallites appear, indicating the formation of Ni grains. As for the samples reduced at 450 and 700 °C, it can be clearly seen that small Ni particles are uniformly distributed in the Al_2O_3 matrix. When comparing Fig. 4(b) with (c) and (d), it is obvious that the number of nano-sized Ni crystallites increases with increasing reduction temperature. In addition, the main grain size increases with increasing reduction temperature, as shown in Fig. 4(b)–(d). The mean grain sizes of Ni particles estimated from TEM images Fig. 4(c) and (d) are consistent with those calculated from XRD analysis, shown in Table 1. These results indicate that the powder reduced at 450 °C is a particularly suitable candidate for use in the catalytic reaction for the production of carbon nanotubes, since the reduction process is 60–70% complete (Fig. 2) and the grain size remains small (around 10 nm).

Fig. 5 shows dark-field images of the reduced powders (MA18 and MA36). Fig. 5(b) confirms that small Ni crystallites are uniformly distributed in the Al_2O_3 matrix. For the reduced powder after mechanical alloying for 18 h, the particle size distribution is not so uniform, with some relatively large particles being found. This result shows that after mechanical alloying for 18 h, Al_2O_3 and NiO are not well mixed. The formation of large Ni particles suggests the possible presence of large NiO particles after the mechanical alloying.

BET analysis

Table 2 shows the specific surface area of the Al_2O_3–Ni powders derived from MA18 and MA36 precursors (S_R). Obviously, the S_R of both nanocomposite powders increases with the reduction temperature. This is contrary to the general belief that S_R should decrease with increasing reduction temperature due to enhanced grain growth, agglomeration and the possible occurrence of sintering. Laurent *et al.* also reported the increase of S_R with increasing reduction temperature.[10] However, in their case, the reduction of the precursors was performed in a flow of H_2–CH_4 (6 mol%) and therefore the increase in S_R was ascribed to the formation of

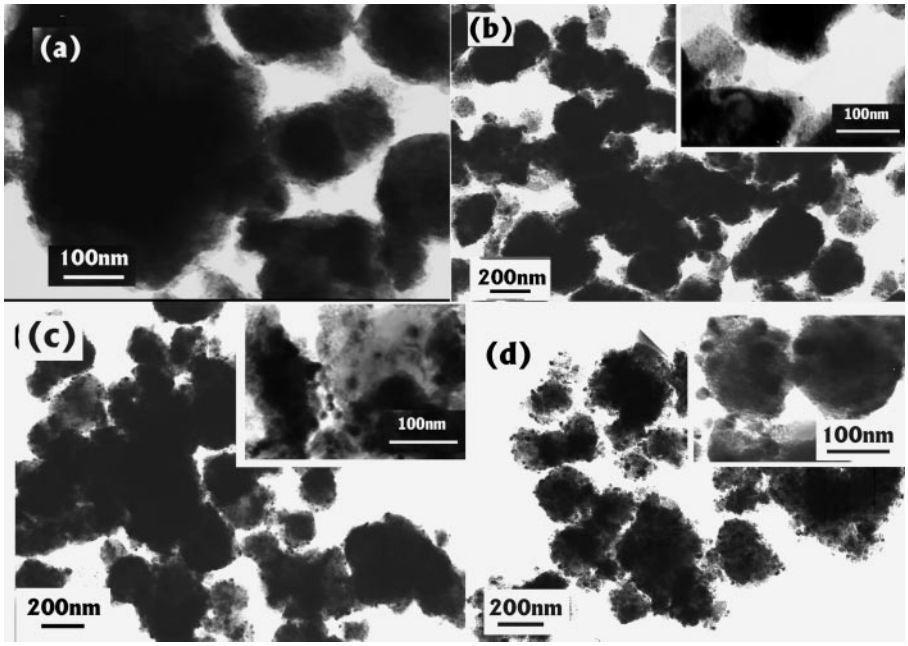

Fig. 4 TEM images of Al_2O_3–Ni composite powders derived from (a) MA36 oxide precursors reduced at (b) 300, (c) 450 and (d) 700 °C.

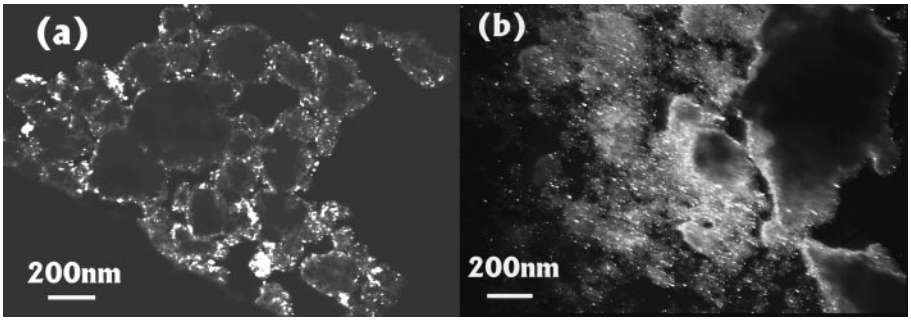

Fig. 5 Dark-field images of the catalytic composite powder reduced at 450 °C: (a) derived from MA18 precursor; (b) derived from MA36 precursor.

carbon species, particularly carbon nanotubes. In our experiment, no hydrocarbon gas was used during reduction, so the increase in S_R must be a result of other factors.

Since the density of the NiO phase is lower than that of the Ni metallic phase, it is conceivable that a reduction in volume occurs with the nucleation and growth of Ni particles. As a result, a large number of pores are produced around newly formed Ni particles. Furthermore, it can be expected that the porosity is greatly increased at high reduction temperatures because of the formation of a large amount of Ni phase converted from NiO phase.

Compared with the sample derived from the MA18 precursor, the Al_2O_3–Ni nanocomposites obtained from the MA36 precursor show larger S_R after reduction at the same temperatures. As mentioned above, in MA36, the size of the NiO particles in the Al_2O_3 matrix is smaller and their distribution is more uniform than those in the MA18 powder. Therefore, a larger number of pores are formed in the MA36 sample. Furthermore, more uniformly dispersed NiO particles also efficiently inhibit coalescence or sintering between the newly formed Ni particles, avoiding the closure of pores. In terms of the above, specific surface area measurements can provide us with another useful method of evaluating the quality of the precursors obtained using the mechanical alloying process.

As can be seen from Table 2, after CH_4 treatment, the specific surface area (S_{CNT}) of all CNT-containing nanocomposites increases due to the formation of carbon species, especially carbon nanotubes. For catalytic powders reduced at 450 and 700 °C and after CH_4 treatment, S_{CNT} increases dramatically relative to S_R. While for catalytic powder reduced at 300 °C, the deposition of carbon resulted in rather small changes in specific surface area. This, once again, suggests that, at 300 °C, only a small amount of NiO is reduced to Ni, giving rise to limited production of CNTs, a fact also indicated by the results of the magnetic measurements.

The growth of carbon nanotubes

To study the influence of different catalysts, two kinds of processes, co-precipitation and mechanical alloying, were employed to produce the catalyst powders as described above. A comparison between the CNTs derived from these two different catalysts reduced at 450 °C indicates the higher efficiency of CNT growth on the mechanical alloying-derived catalyst. As shown by Fig. 6, it is obvious that the yield of CNTs is much higher for the MA36-derived catalyst [Fig. 6(b)] than that for the co-precipitation-derived catalyst [Fig. 6(a)]. In Fig. 6(a), the Al_2O_3 matrix particles are less covered by the web of CNTs, such that their primary surface and edges can be clearly observed, while in Fig. 6(b), the thick web of CNTs makes the nanocomposite particles appear as downy spheres connected with numerous strings of nanofibers. The higher yields for the MA36-derived catalysts can be readily attributed to their higher Ni phase content after reduction, as indicated by the M_s values shown in Fig. 2, though both catalysts and CNT

Table 2 Saturation magnetization (M_s) and specific surface area (S) for MA18 and MA36-derived Al_2O_3–Ni powder and CNT-containing nanocomposites (M_{RS}: M_s of Al_2O_3–Ni powder; M_{CNT}: M_s of CNT-containing nanocomposites; S_R: S of Al_2O_3–Ni powder; S_{CNT}: S of CNT-containing nanocomposites; $\Delta M = M_{RS} - M_{CNT}$; $\Delta S = S_{CNT} - S_R$)

	Reduction temperature/°C	M_{RS}/emu g^{-1}	M_{CNT}/emu g^{-1}	ΔM/emu g^{-1}	C_n/wt%	S_R/m^2 g^{-1}	S_{CNT}/m^2 g^{-1}	ΔS/m^2 g^{-1}	$\Delta S/C_n$/m^2 g^{-1}
MA18	300	1.27	1.26	0.01	0.72	18.73	20.23	1.50	218.1
MA18	450	5.64	4.73	0.91	16.13	28.02	62.41	34.39	213.2
MA18	700	9.97	7.11	2.86	28.71	38.16	87.94	49.78	173.4
MA36	300	1.28	1.27	0.01	1.56	20.11	23.75	3.64	233.3
MA36	450	7.45	5.81	1.64	22.01	32.43	82.70	50.27	228.4
MA36	700	10.80	7.31	3.49	32.31	41.82	109.51	67.69	209.5

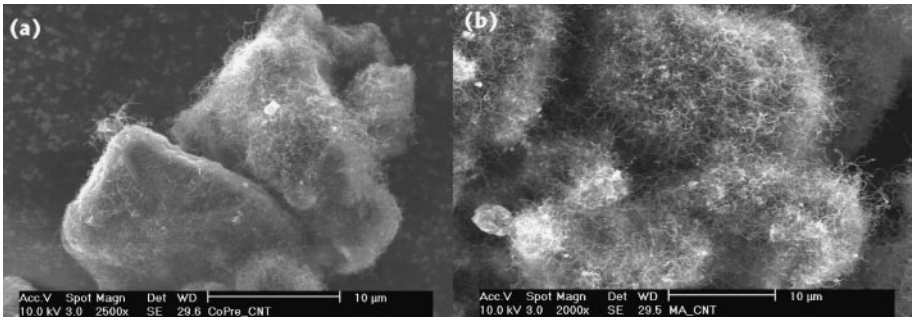

Fig. 6 SEM images of CNT products synthesized from different catalysts reduced at 450 °C: (a) co-precipitation-derived catalyst; (b) MA36-derived catalyst.

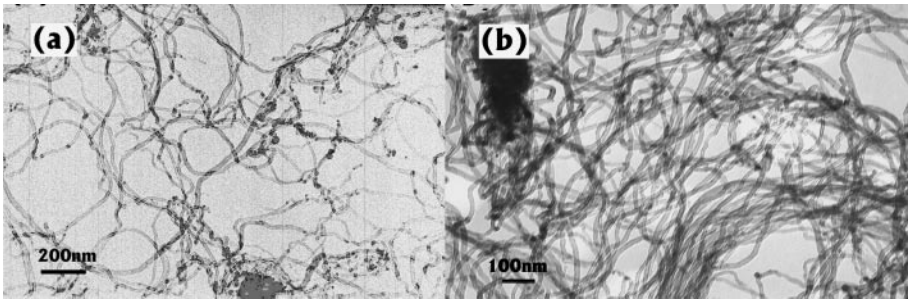

Fig. 7 TEM images of CNT products synthesized with different catalysts reduced at 450 °C: (a) co-precipitation-derived catalyst; (b) MA36-derived catalyst.

products were obtained under the same conditions. The porous structure presumably makes a contribution to the high productivity.

The TEM images in Fig. 7 show the morphology of the CNTs as in Fig. 6(a) and (b). In both cases, the obtained nanotubes appear as rather long and curved multi-walled tubes that are usually bundled together. Also the diameters of these tubes are relatively homogeneous throughout their length and in the range 10–15 nm. For the MA36-derived catalyst, the nanotubes are more abundant and tangled together to form a massive web, which again reflects the difference in the CNT yields for these two kinds of catalysts. This demonstrates that mechanical alloying is a promising process for the production of catalysts for the catalytic growth of carbon nanotubes.

Fig. 8(a) shows a typical TEM image of CNTs grown on the catalyst derived from the MA18 powder reduced at 450 °C. A certain number of irregular or spherical particles of 10–30 nm in size [black dots in Fig. 8(a)] are observed superimposed on the web of nanotubes. These unwanted species are believed to be crystallized and/or amorphous carbon particles as well as carbon-encapsulating Ni particles, according to many reports.[8–10,14,21] For the sample shown in Fig. 7(b) and Fig. 8(b), using the MA36 powder reduced at 450 °C as the catalyst, only a few such deposits can be detected on the web of CNTs. The sole difference between the sample shown in Fig. 8(a) and that in Fig. 8(b), is that the catalyst precursors were milled for 18 and 36 h, respectively. As mentioned above, the shorter mechanical alloying time not only inhibits the refinement of the NiO particles, but might also weaken the binding between NiO and Al_2O_3. Due to the poor refinement of the NiO particles, larger Ni particles result from the reduction. This is definitely unfavorable for the formation of nanotubes, because only sufficiently small metallic particles (usually less than 20 nm in diameter) can lead to nanotubes.[22] As a result, the large particles become favorable sites for the formation of carbon-encapsulating particles, which decreases the yield of nanotubes. On the other hand, due to the weakened binding between NiO and Al_2O_3 in the MA18 powder, the Ni particles are more easily spalled off from the matrix due to the volume shrinkage during reduction. Agglomeration and even sintering might occur because Ni particles are no longer separated by Al_2O_3.

Furthermore, the formation of nickel aluminium oxide solid solution in the MA36 precursor is definitely beneficial to the formation of the extremely small Ni particles. As a result, the *in situ* reduced Ni particles are more uniformly dispersed on the Al_2O_3 matrix and show a reduced tendency to coalesce together compared to those in the MA18-derived catalysts. Therefore, the carbon nanotubes obtained with the MA36-derived catalysts are of higher quality and contain fewer unwanted carbon species.

Such differences in the morphologies of the carbon products can also be evaluated by the ratio of the change in specific surface area (ΔS) to carbon content (C_n) after CH_4 treatment. The criterion $\Delta S/C_n$ is a very useful parameter to assess the quality of nanotubes.[9–15] A higher figure denotes a smaller tube diameter and a greater yield of nanotubes. In this work, the carbon content (C_n) was estimated from the results of magnetic measurements. The principle behind such calculations lies in the fact that the decrease in the saturation magnetization (M_s)

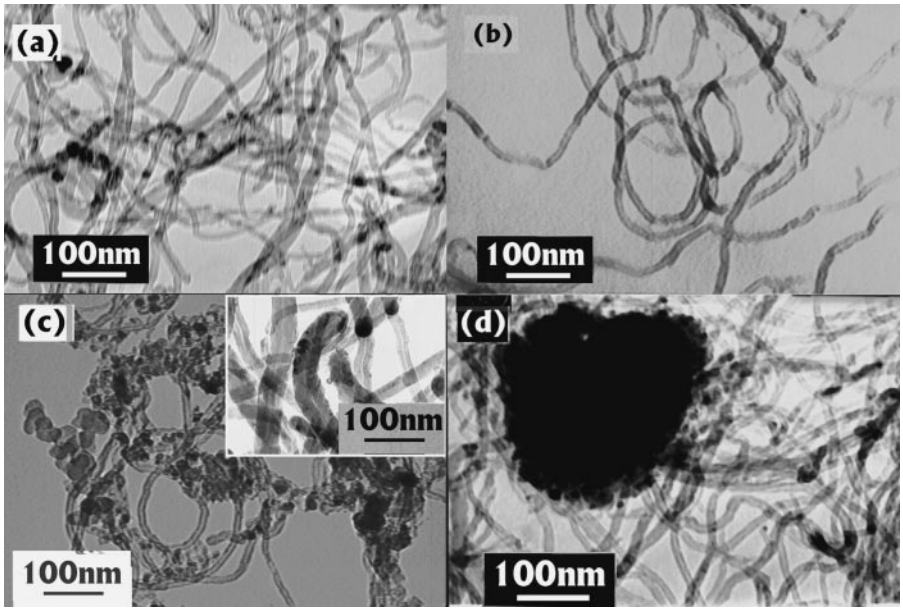

Fig. 8 TEM images of CNTs grown with catalysts derived from different processes: (a) MA18-derived catalyst, reduced at 450 °C; (b) MA36-derived catalyst, reduced at 450 °C; (c) MA18-derived catalyst, reduced at 700 °C; (d) MA36-derived catalyst, reduced at 700 °C.

after CH_4 treatment is due to the formation of carbon products. Therefore, the higher the carbon content, the lower the M_s value. The measured specific surface areas and the calculated carbon contents are listed in Table 2. A comparison of $\Delta S/C_n$ between the CNT-containing MA18 and MA36-derived nanocomposites clearly indicates the difference in CNT quality.

It is also interesting to study the effect of reduction temperature. With increasing reduction temperature, the growth of Ni particles is enhanced. For the MA18-derived catalyst reduced at 700 °C, we observed a much greater number of irregular or spherical particles superimposed on the web of CNTs, as indicated by a comparison between Fig. 8(a) and (c). In addition, a lot of thick-walled nanotubes as well as carbon filaments (20–40 nm in diameter) with irregular shapes are formed, as shown in Fig. 8(c). Furthermore, the diameters of the obtained tubes were no more uniform. For the MA36-derived catalyst, increasing the reduction temperature has less of an effect on the morphologies of the nanotubes than for the MA18-derived catalyst. Though a small number of thick tubes and carbon filaments, as well as nanosized particles, appear in the sample, no apparent change in the yield and morphologies of CNTs was observed under SEM and TEM, as shown by Fig. 8(b) and (d).

Such different behaviors of CNT morphologies for these two kinds of catalysts strongly suggest that the Ni particles in the MA18-derived catalyst are more sensitive to the change in reduction temperature, more easily coarsening than those in the MA36-derived catalyst. This tendency was also reflected by the quality parameter $\Delta S/C_n$, as shown in Table 2. From the $\Delta S/C_n$ values, we can clearly see that the catalysts reduced at lower temperature are more suitable for growth of CNTs with higher $\Delta S/C_n$. However, although the catalysts reduced at 300 °C can generate CNTs with high $\Delta S/C_n$, the productivity is too low. Therefore, the catalysts reduced at an intermediate temperature of 450 °C seem to be the most suitable for CNT synthesis.

Conclusion

Mechanical alloying was employed to prepare the precursors of the catalytic Al_2O_3–Ni powders, from which bulk amounts of multi-walled carbon nanotubes were obtained. It was demonstrated that mechanical alloying-derived catalysts favor higher yields of CNT products in comparison with the co-precipitation-derived catalyst. The higher productivity was ascribed to the higher reducibility and porous structure of the mechanically alloying-derived powders.

Milling time in the mechanical alloying process plays a determinative role in the fabrication of Al_2O_3–Ni nanocomposites and the synthesis of CNTs. Longer mechanical alloying times can result in the dramatic refinement of NiO particles and the formation of nickel aluminium oxide solid solution. This in turn leads to the uniform dispersion of Ni particles on the Al_2O_3 matrix after reduction. As a result, the obtained CNTs are of high quality, as verified by the parameter $\Delta S/C_n$.

References

1 A. C. Dillon, *Nature*, 1997, **386**, 377.
2 G. E. Gadd, *Science*, 1997, **277**, 933.
3 P. J. Britto, K. S. V. Santhanam and P. M. Ajayan, *Nature*, 2000, **406**, 586.
4 P. G. Collins, A. Zettl, H. Bando, A. Thess and R. E. Smalley, *Science*, 1997, **278**, 100.
5 S. Iijima, in *Proc. IEEE Annu. Int. Workshop Micro Electro Mech. Syst.: 11th, 1998*, IEEE, Heidelberg, Germany, 1998, p. 520.
6 H. Dai, J. H. Hafner, A. G. Rinzler, D. T. Colbert and R. E. Smalley, *Nature*, 1996, **384**, 147.
7 A. G. Rinzler, J. H. Hafner, P. Nikolaev, L. Lou, S. G. Kim, D. Tomanek, P. Nordlander, D. T. Colbert and R. E. Smalley, *Science*, 1995, **269**, 1550.
8 Z. Y. Zhong, H. Y. Chen, S. B. Tang, J. Ding, J. Y. Lin and K. L. Tan, *Chem. Phys. Lett.*, 2000, **330**, 41.
9 A. Pelgney, Ch. Laurent and A. Rousset, *J. Mater. Chem.*, 1999, **9**, 1167.
10 Ch. Laurent, A. Pelgney and A. Rousset, *J. Mater. Chem.*, 1998, **8**, 1263.
11 O. Quenard, Ch. Laurent, M. Brieu and A. Rousset, *Nanostruct. Mater.*, 1996, **7**, 497.
12 A. Peigney, Ch. Laurent, F. Dobigeon and A. Rousset, *J. Mater. Res.*, 1997, **12**, 613.
13 E. Flahaut, A. Govindaraj, A. Peigney, A. Rousset and C. N. R. Rao, *Chem. Phys. Lett.*, 1999, **300**, 236.
14 A. Govindaraj, E. Flahaut, Ch. Laurent, A. Peigney, A. Rousset and C. N. R. Rao, *J. Mater. Res.*, 1999, **14**, 2567.
15 E. Flahaut, A. Peigney, Ch. Laurent and A. Rousset, *J. Mater. Chem.*, 2000, **10**, 249.
16 C. C. Koch, *Nanostruct. Mater.*, 1993, **2**, 109.
17 R. B. Schwarz and C. C. Koch, *Appl. Phys. Lett.*, 1986, **49**, 146.
18 J. Ding, W. M. Miao, P. G. McCormick and R. Street, *Appl. Phys. Lett.*, 1995, **67**, 3804.
19 J. Ding, P. G. McCormick and R. Street, *J. Magn. Magn. Mater.*, 1997, **171**, 309.
20 J. Wang, D. M. Wan, J. M. Xue and W. B. Ng, *Adv. Mater.*, 1999, **11**, 210.
21 M. Cassell Alan, A. Raymakers Jeffrey, J. Kong and H. Dai, *J. Phys. Chem. B*, 1999, **103**, 6484.
22 R. T. K. Baker and N. Rodriguez, *Mater. Res. Soc. Symp. Proc.*, 1994, **349**, 251.